
Article:
Farzi, M., Morris, R.M., Penny, J. et al. (5 more authors) (2017) Quantitating the effect of prosthesis design on femoral remodeling using high-resolution region-free densitometric analysis (DXA-RFA). Journal of Orthopaedic Research. ISSN 0736-0266

https://doi.org/10.1002/jor.23536

Research Article

Quantitating the Effect of Prosthesis Design on Femoral Remodeling Using High-Resolution Region-Free Densitometric Analysis (DXA-RFA) †

Mohsen Farzi, MSc [1,3]; Richard M Morris, BMedSci [1]; Jeannette Penny, MD, PhD [2]; Lang Yang, PhD [1]; Jose M Pozo, PhD [3]; Søren Overgaard, MD, PhD [2]; Alejandro F Frangi, PhD [3]; J Mark Wilkinson, MB ChB, PhD [1]

[1] University of Sheffield, Academic Unit of Bone Metabolism, Northern General Hospital, Sheffield, UK.
[2] University of Southern Denmark, Institute of Clinical Research, Department of Orthopaedic Surgery and Traumatology, Odense University Hospital, Odense, Denmark.
[3] Centre for Computational Imaging & Simulation Technologies in Biomedicine (CISTIB), Department of Electronic and Electrical Engineering, Sheffield, UK.

Running title: DXA-RFA and femoral periprosthetic bone remodeling

*Corresponding author: Prof J Mark Wilkinson, Department of Oncology and Metabolism, University of Sheffield, The Medical School, Beech Hill Road, Sheffield, S10 2RX, United Kingdom
Email: j.m.wilkinson@sheffield.ac.uk
Telephone +44 114 271 4705
Fax +44 114 2618775

Author Contributions Statement: Research design (MF, AFF, JMW); data acquisition (JP, SO, JMW); data analysis (MF, RMM, LY, JMP, AFF, JMW); drafting of the paper and critical revisions (all).

Additional Supporting Information may be found in the online version of this article.

Received 22 November 2016; Revised 9 January 2017; Accepted 2 February 2017
Journal of Orthopaedic Research

DOI 10.1002/jor.23536

ABSTRACT

Dual energy X-ray absorptiometry (DXA) is the reference standard method used to study bone mineral density (BMD) after total hip arthroplasty (THA). However, the subtle, spatially-complex changes in bone mass due to strain-adaptive bone remodeling relevant to different prosthesis designs are not readily resolved using conventional DXA analysis. DXA region free analysis (DXA RFA) is a novel computational image analysis technique that provides a high-resolution quantitation of periprosthetic BMD. Here we applied the technique to quantitate the magnitude and areal size of periprosthetic BMD changes using scans acquired during two previous randomized clinical trials (2004 to 2009); one comparing three cemented prosthesis design geometries, and the other comparing a hip resurfacing versus a conventional cementless prosthesis. DXA RFA resolved subtle differences in magnitude and area of bone remodeling between prosthesis designs not previously identified in conventional DXA analyses. A mean bone loss of 10.3%, 12.1%, and 11.1% occurred for the three cemented prostheses within a bone area fraction of 14.8%, 14.4%, and 6.2%, mostly within the lesser trochanter ($P<0.001$). For the cementless prosthesis, a diffuse pattern of bone loss (-14.3%) was observed at the shaft of femur in a small area fraction of 0.6% versus no significant bone loss for the hip resurfacing prosthesis ($P<0.001$). BMD increases were observed consistently at the greater trochanter for all prostheses except the hip-resurfacing prosthesis, where BMD increase was widespread across the metaphysis ($P<0.001$). DXA RFA provides high-resolution insights into the effect of prosthesis design on the local strain environment in bone.

Key words: Hip Arthroplasty, Bone mineral density, Strain-adaptive bone remodeling, Dual energy X-ray absorptiometry (DXA), False discovery rate (FDR)

This article is protected by copyright. All rights reserved

Introduction

Prosthesis design influences the local mechanical environment of the proximal femur after total hip arthroplasty (THA), resulting in strain-adaptive bone remodeling [1–3]. Several factors influence the extent of bone loss that occurs around different prosthesis types; including prosthesis geometry, material stiffness, method of fixation, and surface coating [4–10]. Periprosthetic bone loss is a risk factor for fracture and causes reconstruction challenges at revision surgery [11,12]. Dual energy X-ray absorptiometry (DXA) is the reference standard method used to study bone mineral density (BMD) after THA [13,14]. However, the resolution of conventional DXA analysis is a limiting factor as spatial information is lost by pooling pixels into a small number of pre-defined regions of interest (ROIs) [15,16] that substantially limit the precise localization and quantitation of BMD change events. This data averaging also leads to inconsistent results for a given dataset depending on the number and placement of the analysis ROIs [5,15,17–20].

There is a need for high resolution, low radiation exposure technologies for evaluating the bone architectural changes associated with different biomaterial designs and implant geometries [21]. Such technologies would facilitate the non-invasive clinical assessment of novel prostheses that aim to better mimic the natural loading environment, or have surface coatings that aim to modulate the biology of the local bone environment [22]. We recently reported a high-resolution computational method for DXA scan analysis, termed DXA region free analysis (RFA) [23]. DXA RFA applies current advances in image processing, non-rigid registration, and statistical parametric mapping to quantitate BMD at the individual pixel-level [24–26]. The DXA RFA method enables quantitation of the areal size and the anatomic position of regions with statistically significant BMD change without imposing any a-priori assumptions on the analysis region of interest. To this end, we have extended the DXA RFA tool to control for statistical error rates in multiple tests using the False Discovery Rate method (FDR) to enable comparative inferences to be drawn [27]. This approach has previously been applied to femoral

cortical bone analysis using quantitative computed tomography images [28], in functional neuroimaging [29], and in similarly large datasets in other fields [30,31].

Here we applied the extended DXA RFA method to examine the impact of prosthesis design on strain-adaptive bone remodeling in the setting of two previously reported clinical trials using substantially different femoral prosthesis designs [32,33]. In one trial, we compared three different geometries of cemented femoral prosthesis, the Charnley (DePuy International, Leeds, UK), Exeter (Stryker, Newbury, UK), and the C-Stem (DePuy International, Leeds, UK). These prostheses may be classified as shape-closed or force-closed designs [34,35]. Shape-closed designs, like the Charnley, use a bonded prosthesis-cement interface to fix the stem within the cement mantle, acting as a composite-beam, and transfer load to the femur mainly at the level of femoral diaphysis. Force-closed designs, such as the double-tapered (Exeter) and triple-tapered (C-Stem) prostheses, have a non-bonded prosthesis-cement interface, where the stem acts as a mobile wedge within the cement mantle [34,36]. This allows initial distal migration to set up hoop stresses in the proximal cement mantle resulting in more proximal load transfer between the femoral prosthesis and the host bone [37]. In the other trial, we compared bone remodeling around a hip resurfacing prosthesis versus a conventional cementless total hip replacement. The load transfer pattern in RHR occurs directly from the femoral head to the metaphysis, and is thought to be more representative of that found in the native proximal femur than that for a conventional stemmed prosthesis [20,38–41].

Materials and methods

Study populations and scan acquisitions

Anonymized DXA scans from two previous ethically approved clinical trials, for which written, informed consent was provided, were examined using DXA RFA [32,33]. All subjects underwent surgery for idiopathic or secondary osteoarthritis, and were free from use of drugs known to affect BMD. All scans were acquired using a Hologic QDR 4500A fan-beam densitometer (Hologic Inc., Bedford, MA), using the ‘metal removal hip’ scanning mode with a point resolution of 0.6mm and a line spacing of

1.1mm. Scans were performed with the subject in the supine position with the legs in neutral rotation and full extension. Scan acquisition was started approximately 2.5cm distal to the tip of the femoral prosthesis, with the longitudinal axis of the prosthesis shaft vertical and occupying the center of the scan field. The scan was continued proximally until 2cm above the tip of the greater trochanter [15].

Study designs and subject monitoring

FDR validation: To investigate the accuracy of FDR algorithm incorporation into the DXA RFA framework, we examined sequential DXA scans taken on the same day after repositioning in 17 men (mean age 50 years, range 33 to 67) and 12 women (mean age 53 years, range 35 to 61). Scans were acquired a mean of 6 months (SD 3) after THA[15]. The hypothesis tested here was that we expected no significant differences in measured pixel-level BMD between the individual scan pairs at FDR level of 0.05.

The effect of cemented stem design on bone remodeling: The subjects in this study were randomized at a ratio of 1:1:1 to receive either a cemented composite-beam prosthesis (Charnley, DePuy Synthes Ltd, n=35), a double-tapered prosthesis (Exeter, Stryker UK Ltd, n=38), or a triple-tapered prosthesis (C-stem, DePuy Synthes Ltd, n=38) [32]. All patients were mobilized with unrestricted weight bearing on the first or second post-operative days. BMD was measured at post-operative baseline within 1 week of surgery, and at 3, 6, 12 and 24 months later using the same Hologic densitometer.

Effect of hip resurfacing versus cementless THA on bone remodeling: The subjects in this study were randomized at a ratio of 1:1 to receive either a hip resurfacing prosthesis (Articular Surface Replacement (ASR) total femoral prosthesis, DePuy Synthes Ltd, n=13) or THA using a cementless, proximally plasma-coated, titanium femoral component (Bi-metric, Biomet, Bridgend, UK, n=17) [33]. All patients were mobilized full weight bearing on the first or

second post-operative days. BMD was measured at post-operative baseline within 1 week of surgery, and at 2, 12 and 24 months later using the same Hologic densitometer.

Scan analysis

The DXA-RFA method was based upon a proprietary DXA bone map extraction algorithm APEX 3.2 (Hologic Inc, Waltham, MA), and implemented in Matlab v7.11.0.584 r2010b (Mathworks Inc, Cambridge, MA), and performed as previously described [23].

Image segmentation: Briefly, for each Hologic prosthetic hip scan BMD image of the proximal femur was extracted from the 2 archived Hologic scan files using DXA-RFA (.p and .r files, approximately 14,000 pixels per scan; mean pixel size 0.56x0.56mm^2).The extracted images were then segmented into prosthesis, bone, and soft tissue compartments using edge-detection, intensity thresholding, and morphological operations. Subsequently, the pixel BMD values within the bone compartment were computed using DXA-RFA.

Image alignment and template registration: Anatomic landmark and control points were defined automatically for each DXA scan, as previously described [23]. Next, separate scan templates were generated for each prosthesis type using the Generalized Procrustes algorithm [42]. For each prosthesis type, the individual scans were registered to the corresponding template using a thin plate spline (TPS) algorithm [26].

Baseline analysis: The baseline demographic characteristics of the subjects between each of the prosthesis groups were compared using the χ^2 test, Fisher's exact test, the Mann-Whitney U test, or Student's t-test, as appropriate. The mean distribution of pixel BMD values among the post-operative baseline scans was computed for each prosthesis.

False Discovery Rate analysis: The pixel-level BMD changes with respect to the baseline measurement were examined using a paired t-test at each time-point. Next, to address the multiple testing issue, the FDR was controlled using the Benjamini and Hochberg approach [43].

In this approach, the acceptable rate α is defined beforehand (here at 0.05) and the corresponding p-value threshold is then estimated. This method selects the set of pixels with significant BMD change at FDR level α, yet does not provide corrected p-values for each pixel. The FDR analogue to the p-value is called q-value. The q-value of a pixel is the minimum FDR level α for which this pixel is selected as significant. The mapping from p-values to q-values is obtained as follows. First, the p-values are sorted increasingly as $p_{(1)}, \leq p_{(2)} \leq \cdots \leq p_{(N)}$. The corresponding q-values are then given by $q_{(i)} = p_{(i)} * \frac{N}{i}$.

All pixels with $q \leq 0.05$ were selected as statistically significant. The areal size of regions with significant BMD change was quantitated as the fraction of periprosthetic bone area, i.e. the number of pixels with $q \leq 0.05$ divided by the number of all pixels in the template. The areal proportions were then compared between prosthesis designs using a chi-squared test. The pixel-level FDR q-values were also rendered as heat-maps to denote the anatomic location of significant BMD change events within the bone.

Results

FDR validation

Fig. 1A shows the P-P plot for the repositioned scans examined here. A P-P plot is a diagram of increasingly sorted observed p-values against the $i/(N+1)$ quantile of the uniform distribution, where N is the total number of observed p-values. Under null hypothesis, the expected curve in the P-P plot is the diagonal line of identity. Large deviations from this diagonal have lower probability. As shown in Fig. 1A, the P-P plot follows the line of identity. This means that no pixels with significant BMD change were identified across all pixels in the 29 subject pairs, confirming the null hypothesis. In comparison, Fig. 1B shows the P-P plot for the Charnley prosthesis after 24 months as an example where the null hypothesis is rejected, since the P-P plot deviates below the slope-α line (Fig. 1C).

Clinical trial subject characteristics

The participants within each clinical trial were of similar age, sex distribution, and body mass index (Table 1). The subjects participating in the cemented stem geometry trial were older than those participating in the conventional cementless femoral prosthesis versus hip resurfacing trial (71±6 versus 57±6, P<0.001), and a greater proportion were female (53:58 versus 22:8, P=0.013). The BMI of participants in each study were 29.2±4.4 versus 28.3±4.4, respectively (P=0.397).

Post-operative baseline mean BMD distribution

Baseline scans for all prosthesis groups showed a pattern of mean BMD distribution consistent with proximal femoral architecture with differentiation of cancellous versus cortical bone (Figure 2). Areas of lowest BMD (approximately 0.5 to 1g/cm^2) were observed in the cancellous bone within the greater and lesser trochanter. BMD was highest (2-3g/cm^2) in the cortical bone of the femoral diaphysis. Subjects with cemented prostheses showed highest bone mass in the region of cementation, with a measured BMD of up to 4g/cm^2.

Effect of cemented stem design on bone remodeling

Some common remodeling features were observed across all the cemented prosthesis designs over the 24-month trial periods. Figs. 3a to 3c show the magnitude of pixel BMD change (%) at 24 months, and Figs. 4a to 4c show the corresponding FDR q maps. The percentage bone areas over which a significant change in BMD was observed for each prosthesis by 24 months are shown in Table 2.

BMD change events occurred in discrete focal areas. An increase in bone mass was observed consistently in the greater trochanter area, a site of multiple tendinous attachments. Here, an average BMD increase of 32.1% within 16.6% of the periprosthetic bone area was observed for the cemented composite beam (Charnley) prosthesis, 31.2% within 9.7% of the area for the cemented sliding double-taper (Exeter) prosthesis, and 34.5% within 6.5% of the area for the cemented sliding triple-taper (C-stem) prosthesis was observed at 24 months ($q \leq 0.05$ all comparisons). The areal proportions associated with bone gain were significantly different between the three cemented designs ($p<0.001$).

An average bone loss of 10.3%, 12.1%, and 11.1% within an area of size 14.8%, 14.4%, and 6.2% was observed for the Charnley, Exeter, and C-stem prostheses, respectively ($q \leq 0.05$), mostly at the lesser trochanter. The areal proportions associated with bone loss were also significantly different between the three cemented designs ($p < 0.001$). The greatest BMD changes occurred in the metaphyseal region for all cemented prosthesis designs, with relatively less change at the femoral diaphysis.

Bone remodeling patterns were both rate and location specific to each prosthesis design (supplementary Figs 1 to 3). No significant BMD change was observed at any pixel at 3 months for the Charnley prosthesis. However, an average BMD increase of 12.7% was observed within a small fraction (0.7%) of the periprosthetic bone area for the C-stem prosthesis at this time-point ($q \leq 0.05$), and bone loss of 6.8% over 7% of the bone area medial to the Exeter prosthesis ($q \leq 0.05$). When we stratified the dataset by subject sex to determine whether this was a significant covariate, we observed a trend towards smaller areas of bone loss and lower magnitude of bone loss in men versus women across the cemented prosthesis designs (Supplementary table 1).

Effect of hip resurfacing versus cementless THA on bone remodeling

An average BMD increase of 35.9% over an area of 22.3% was observed locally at the greater trochanter for the Bi-metric prosthesis (Fig 3d and Fig 4d; $q \leq 0.05$). A diffuse pattern of bone loss (-14.3%) was also observed at the shaft of femur for Bi-metric prosthesis at 24 months over a small fraction of periprosthetic bone area (0.6%). No periprosthetic bone loss was observed around the hip resurfacing prosthesis at 24-months (Fig 3e and Fig 4e). However, an average BMD increase of 34.3% was observed over 30.7% of the proximal femoral metaphysis ($q \leq .05$). The areal proportions associated with bone gain were significantly different between the hip resurfacing prosthesis and the cementless hip replacement technique ($p < 0.001$).

The contrasting patterns of focal trochanteric versus widespread metaphyseal increase in BMD for the Bi-metric versus ASR prostheses was apparent by 12 months, and persisted at 24 months

(Supplementary Figs 4 and 5). The increase in bone mass around the ASR prosthesis was observed over the whole proximal femoral metaphysis, but was most densely concentrated in the bone adjacent to the lateral border of the prosthesis and greater trochanter. For the comparison between hip resurfacing versus the cementless THA, the number of women in both prosthesis groups was too small to allow a meaningful stratified analysis by sex.

Discussion

We analyzed BMD changes around five different prosthesis designs using DXA RFA with FDR to demonstrate in high resolution the effect that different prosthesis designs have on proximal femoral strain-adaptive remodeling. This approach is widely clinically-applicable, non-invasive and associated with low radiation exposure. We observed some remodeling features that were common around all prosthesis, and others that were design-specific. Our finding that remodeling events occurred in small but spatially discrete 'quanta' is consistent with the concept that post-operative bone remodeling occurs in discrete multicellular units [44,45]. The observation that periprosthetic bone remodeling events are spatially complex, heterogeneous, and vary in density distribution with prosthesis design supports finite element analysis predictions [46]. It is also consistent with the view that the conventional ROI-based approach results in substantial data loss that impacts interpretation [15].

Consistently across all prosthesis designs, we found a gain in bone mass in the region of the greater trochanter, albeit this increase in bone mass was most widely distributed for the hip resurfacing group. Hip resurfacing was also the only prosthesis design around which increased bone mass occurred within the cortical bone of the proximal medial femur. This aligns with finite element predictions of the stress-redistribution at the femoral neck induced by this prosthesis class [47,48]. We have previously identified a similar BMD trend using conventional DXA [33], however, analysis using DXA RFA enabled precise localization of the magnitude and area of these events. Although these data support the concept that head resurfacing prosthesis induce load transfer at the metaphyseal level, the approach does not

quantitate over the studied timeframe the possible influence of adverse responses to metal debris on the local tissue microenvironment.

Previous conventional analysis using the seven Gruen zones showed that the greatest bone loss occurred in R7 and R6 over 2 years for the three cemented designs [32]. While DXA RFA analysis also showed significant bone loss adjacent to the prosthesis at lesser trochanter (Fig 4a-c), this was more precisely resolved using the technique. Small areas of bone gain at the tendon-bone interface of the lesser trochanter were also observed (Fig 3a-c). In conventional DXA analysis, this spatial information is lost due to the averaging pixels into regions of interest. Moreover, this averaging may cancel out the bone loss with the bone gain in a region. The data for the cemented prostheses stratified by subject sex also suggested a smaller magnitude of bone loss and over a small periprosthetic area in men versus women. However, the subject numbers for this comparison were small and should be interpreted with caution. For the hip resurfacing prosthesis, the conventional analysis showed a bone gain in all the Gruen zones [33]. This is compatible with spatial BMD change patterns in Fig 3e, where these changes are anatomically observed in the femoral shaft. The number of women in the cementless THA versus hip resurfacing study was <10, and a gender-specific comparison was not performed.

The incorporation of FDR into the DXA RFA framework enabled quantitation of the architectural details of femoral bone mass distribution and robust statistical analysis of BMD change events. These changes were also rendered as heat-maps for visual assessment. The FDR algorithm was applied to limit the proportion of false positives among statistically significant results. This primary concern is not directly addressed with Bonferroni-type adjustments [31,43]. Moreover, the FDR approach gives increased statistical power in comparison with the methods that control family-wise error rate [31,43]. The validation of the FDR correction on the set of 29 repositioned scans confirmed the reliability of the method when applied in the DXA RFA framework.

The DXA RFA analysis approach is also subject to limitations. The method provides a two dimensional representation of three-dimensional events. However, this is a limitation of DXA per-se rather than this analysis solution, the principle of which may be applied equally to cross-sectional imaging as to planar images. DXA RFA uses a template to create an average representation of the femoral anatomy within the study population. We have previously shown that this approach does not affect substantially the precision or accuracy of the tool for femoral bone analyses [23].

In conclusion, the DXA-RFA analysis approach shows that bone remodeling after prosthesis insertion occurs in discrete focal quanta that are spatially-complex and prosthesis-specific. This approach provides a low-radiation exposure method for the radiographic assessment of novel prosthesis designs in the clinical setting, and an opportunity to better enable comparisons between densitometry data, *in-vivo* and *in-silico* biomechanical tools, and other analytical methodologies.

Acknowledgment

This study was funded internally by the University of Sheffield. M Farzi was funded through a PhD Fellowship from the MRC Arthritis Research-UK Centre for Integrated research into Musculoskeletal Ageing (CIMA). The funding source played no role in the investigation

Appendix

Five images showing the BMD change patterns at intermediate time-points associated with each prosthesis are available with the online version of this article as a data supplement.

References

1. Kerner J, Huiskes R, van Lenthe GH, et al. 1999. Correlation between pre-operative periprosthetic bone density and post-operative bone loss in THA can be explained by strain-adaptive remodelling.J Biomech 32(7):695–703.
2. Frost HM. 2001. From Wolff's law to the Utah paradigm: insights about bone physiology and its clinical applications.Anat. Rec. 262(4):398–419.
3. Maistrelli GL, Fornasier V, Binnington A, et al. 1991. Effect of stem modulus in a total hip arthroplasty model.J. Bone Joint Surg. Br. 73–B(1):43–46.
4. Hughes SS, Furia JF, Smith P, Pellegrini V. 1995. Atrophy of the proximal part of the femur after total hip arthroplasty without cement.J Bone Jt. Surg 77–A(2):231–239.
5. Kilgus DJ, Shimaoka EE, Tipton JS, Eberle RW. 1993. Dual-energy x-ray absorptiometry measurement of bone mineral density around porous-coated cementless femoral implants.J Bone Jt. Surg 75–B(2):279–287.
6. Rosenthall L, Bobyns DJ, Tanzer M. 2000. Periprosthetic bone densitometry of the hip: Influence of prosthetic design and hydroxyapatite coating on regional bone remodelling.J Musculoskel Neuron Interact 1:57–60.
7. Karrholm J, Anderberg C, Snorrason F, et al. 2002. Evaluation of a femoral stem with reduced stiffness. A randomized study with use of radiostereometry and bone densitometry.J Bone Jt. Surg 84–A(9):1651–1658.
8. Rahmy AI, Gosens T, Blake GM, et al. 2004. Periprosthetic bone remodelling of two types of uncemented femoral implant with proximal hydroxyapatite coating: a 3-year follow-up study addressing the influence of prosthesis design and preoperative bone density on periprosthetic bone loss.Osteoporos. Int 15(4):281–289.
9. Wilkinson JM, Little DG. 2011. Bisphosphonates in orthopedic applications.Bone 49(1):95–102.
10. Diegel PD, Daniels AU, Dunn HK. 1989. Initial effect of collarless stem stiffness on femoral bone strain.J Arthroplast. 4(2):173–178.
11. Sheth NP, Nelson CL, Paprosky WG. 2013. Femoral bone loss in revision total hip arthroplasty: evaluation and management.J. Am. Acad. Orthop. Surg. 21(10):601–612.
12. Cook RE, Jenkins PJ, Walmsley PJ, et al. 2008. Risk factors for periprosthetic fractures of the hip: a survivorship analysis.Clin. Orthop. Relat. Res. 466(7):1652–1656.
13. Kroger H, Miettinen H, Arnala I, et al. 1996. Evaluation of periprosthetic bone using dual-energy x-ray absorptiometry: Precision of the method and effect of operation on bone mineral density.J Bone Min. Res 11(10):1526–1530.
14. Trevisan C, Bigoni M, Cherubini R, et al. 1993. Dual x-ray absoptiometry for the evaluation of bone density from the proximal femur after total hip arthroplasty: Analysis protocols and reproducibility.Calcif Tissue Int 53:158–161.
15. Wilkinson JM, Peel NFA, Elson RA, et al. 2001. Measuring bone mineral density of the pelvis and proximal femur after total hip arthroplasty.J. Bone Joint Surg. Br. 83(2):283–288.
16. Watts NB. 2004. Fundamentals and pitfalls of bone densitometry using dual-energy X-ray absorptiometry (DXA).Osteoporos. Int. 15(11):847–854.
17. Kiratli BJ, Checovich MM, McBeath AA, et al. 1996. Measurement of bone mineral density by dual-energy x-ray absorptiometry in patients with the Wisconsin hip, an uncemented femoral stem.J Arthroplast. 11(2):184–193.
18. Albanese C V, Santori FS, Pavan L, et al. 2009. Periprosthetic DXA after total hip arthroplasty with short vs. ultra-short custom-made femoral stems: 37 patients followed for 3 years.Acta Orthop. 80(3):291–297.
19. Lerch M, Kurtz A, Stukenborg-Colsman C, et al. 2012. Bone remodeling after total hip arthroplasty with a short stemmed metaphyseal loading implant: finite element analysis validated by a prospective DEXA investigation.J. Orthop. Res. 30(11):1822–1829.
20. Kishida Y, Sugano N, Nishii T, et al. 2004. Preservation of the bone mineral density of the femur after surface replacement of the hip.J. Bone Joint Surg. Br. 86–B(2):185–189.
21. Puleo D a., Nanci A. 1999. Understanding and controlling the bone-implant interface.Biomaterials 20(23–24):2311–2321.
22. Ebramzadeh E, Normand PL, Sangiorgio SN, et al. 2003. Long-term radiographic changes in cemented total hip arthroplasty with six designs of femoral components.Biomaterials 24(19):3351–3363.
23. Morris RM, Yang L, Martín-Fernández MA, et al. 2015. High-Spatial-Resolution Bone Densitometry with Dual-Energy X-ray Absorptiometric Region-free Analysis.Radiology 274(2):532–539.
24. Crum WR, Hartkens T, Hill DLG. 2004. Non-rigid image registration: Theory and practice.Br. J. Radiol. 77(SPEC. ISS. 2):140–153.
25. Ashburner J. 2009. Computational anatomy with the SPM software.Magn. Reson. Imaging 27(8):1163–1174.
26. Rohr K, Stiehl HS, Sprengel R, et al. 2001. Landmark-based elastic registration using approximating thin-plate splines.Med. Imaging, IEEE Trans. 20(6):526–534.
27. Storey J. 2003. The positive false discovery rate: a Bayesian interpretation and the q-value.Ann. Stat. :2013--2035.
28. Li W, Kornak J, Harris T, et al. 2009. Identify fracture-critical regions inside the proximal femur using statistical parametric mapping.Bone 44(4):596–602.
29. Genovese C, Lazar N, Nichols T. 2002. Thresholding of statistical maps in functional neuroimaging using the false

discovery rate.Neuroimage 15(4):870--878.
30. Jung S-H, Sohn I. 2014. Statistical Issues in the Design and Analysis of nCounter Projects.Cancer Inform. 13(Suppl 7):35–43.
31. Glickman ME, Rao SR, Schultz MR. 2014. False discovery rate control is a recommended alternative to Bonferroni-type adjustments in health studies.J. Clin. Epidemiol. 67(8):850–7.
32. Jayasuriya RL, Buckley SC, Hamer AJ, et al. 2013. Effect of sliding-taper compared with composite-beam cemented femoral prosthesis loading regime on proximal femoral bone remodeling: a randomized clinical trial.J. Bone Joint Surg. Am. 95A(1):19–27.
33. Penny JO, Brixen K, Varmarken JE, et al. 2012. Changes in bone mineral density of the acetabulum, femoral neck and femoral shaft, after hip resurfacing and total hip replacement: two-year results from a randomised study.J. Bone Joint Surg. Br. 94B(8):1036–44.
34. Scheerlinck T, Casteleyn P-P. 2006. The design features of cemented femoral hip implants.J. Bone Joint Surg. Br. 88(11):1409–18.
35. Huiskes R, Verdonschot N, Nivbrant B. 1998. Migration, stem shape, and surface finish in cemented total hip arthroplasty.Clin. Orthop. Relat. Res. 355:103--112.
36. Alfaro-Adrián J, Gill HS, Murray DW. 1999. Cement migration after THR. A comparison of charnley elite and exeter femoral stems using RSA.J. Bone Joint Surg. Br. 81(1):130–134.
37. Shen G. 1998. Femoral stem fixation. An engineering interpretation of the long-term outcome of Charnley and Exeter stems.J. Bone Joint Surg. Br. 80(5):754–6.
38. Hayaishi Y, Miki H, Nishii T. 2007. Proximal femoral bone mineral density after resurfacing total hip arthroplasty and after standard stem-type cementless total hip arthroplasty, both having similar neck preservation and the same articulation type.J. Arthroplasty 22(8):1208–1213.
39. Smolders JMH, Hol A, Rijnders T, van Susante JLC. 2010. Changes in bone mineral density in the proximal femur after hip resurfacing and uncemented total hip replacement: A prospective randomised controlled study.J. Bone Joint Surg. Br. 92(11):1509–14.
40. Cooke NJ, Rodgers L, Rawlings D, et al. 2009. Bone density of the femoral neck following Birmingham hip resurfacing.Acta Orthop. 80(6):660–665.
41. Cordingley R, Kohan L, Ben-Nissan B. 2010. What happens to femoral neck bone mineral density after hip resurfacing surgery?J. Bone Joint Surg. Br. 92(12):1648–53.
42. Goodall C. 1991. Procrustes methods in the statistical analysis of shape.J. R. Stat. Soc. Ser. B 53:285–339.
43. Benjamini Y, Hochberg Y. 1995. Controlling the false discovery rate: a practical and powerful approach to multiple testing.J. R. Stat. Soc. Ser. B :289--300.
44. Kular J, Tickner J, Chim SM, Xu J. 2012. An overview of the regulation of bone remodelling at the cellular level.Clin Biochem 45(12):863–873.
45. Wilkinson JM, Eagleton AC, Stockley I, et al. 2005. Effect of pamidronate on bone turnover and implant migration after total hip arthroplasty: a randomized trial.J. Orthop. Res. 23(1):1–8.
46. Shim VB, Pitto RP, Anderson IA. 2012. Quantitative CT with finite element analysis: towards a predictive tool for bone remodelling around an uncemented tapered stem.Int Orthop 36(7):1363–1369.
47. Taylor M. 2006. Finite element analysis of the resurfaced femoral head.Proc Inst Mech Eng H 220(2):289–297.
48. Watanabe Y, Shiba N, Matsuo S, et al. 2000. Biomechanical study of the resurfacing hip arthroplasty: finite element analysis of the femoral component.J Arthroplast. 15(4):505–511.

Cemented femoral stem geometry study				
Characteristic	Charnley (n=35)	C-stem (n=38)	Exeter (n=38)	P-Value
Age at surgery (years)	70±6	71±7	71±6	[a]0.929
Sex (M:F)	14:21	19:19	20:18	[c]0.527
BMI (Kg/m^2)	28.9±4.6	29.2±4.8	29.3±3.9	[a]0.914

Cementless stemmed versus hip resurfacing study			
Characteristic	Hip resurfacing (n=13)	Cementless stem (n=17)	P value
Age at surgery (years)	57±6	56±6	[b]0.320
Sex (M:F)	8:5	14:3	[d]0.201
BMI (Kg/m^2)	28.0±5.9	28.6±3.0	[b]0.680

Table 1. Characteristics of the patient populations participating in the DXA RFA analyses. Continuous data are presented as mean ± standard deviation, and analysis is between groups within each study using [a]ANOVA or [c]Mann-Whitney test. Categorical data were analyzed using the [b]chi-squared or [d]Fisher's exact test.

	Total		Increased BMD		Decreased BMD	
	Area size (%)	Average BMD (%)	Area size (%)	Average BMD (%)	Area size (%)	Average BMD (%)
Charnley	31.4	12.2	16.6[c]	32.1	14.8	-10.3
Exeter	24.1	5.3	9.7[c]	31.2	14.4	-12.1
C-stem	12.7	12.1	6.5[c]	34.5	6.2	-11.1

Table 2: Area size of regions with significant pixel BMD change (q≤0.05) with corresponding mean BMD change for 3 cemented prosthesis designs over 24 months. The area sizes are expressed as a percentage of the total area of periprosthetic bone in the template image. The average BMD change values are also expressed as a percentage of the baseline BMD value. Area of increased BMD comparison between prosthesis designs by chi-squared test with post-hoc correction. [a]P<0.05, [b]P<0.01, [c]P<0.001.

	Total		Increased BMD		Decreased BMD	
	Area size (%)	Average BMD (%)	Area size (%)	Average BMD (%)	Area size (%)	Average BMD (%)
Cementless stem	22.9	34.6	22.3	35.9	0.6	-14.3
Hip resurfacing	30.7	34.3	30.7	34.3	0.0	0.0

Table 3: Area size of regions with significant pixel BMD change (q≤0.05) with corresponding mean BMD change for a conventional cementless femoral prosthesis (Bi-metric) versus a hip resurfacing femoral prosthesis (ASR) over 24 months. The area sizes are expressed as a percentage of the total area of periprosthetic bone in the template image. The average BMD change values are also expressed as a percentage of the baseline BMD value.

FIGURE LEGENDS

Figure 1: **P-P plot for FDR analysis.** (a) The P-P plot for the set of 29 repositioned pairs of scans. As shown, the blue line almost perfectly follows the diagonal line of identity indicating that the null hypothesis of no change is valid in all pixels. (b) The P-P plot for Charnley prosthesis after 24 months. The blue line deviates below the line of identity, indicating the rejection of null hypothesis. All pixels below the slope-α line corresponding with p-value less than 0.012 are statistically significant at $\alpha = 0.05$.

Figure 2: Mean pixel BMD distribution. The mean distribution of pixel BMD values at baseline measurement is shown for (a) composite-beam (Charnley), (b) double-taper (Exeter), (c) triple-taper (C-stem), (d) Bi-Metric total hip replacement, and (e) ASR hip resurfacing prosthesis designs, respectively.

Figure 3: Longitudinal mean pixel BMD change over 24 months. The pixel BMD change after 24 months is expressed as a percentage of the baseline measurement. The mean distribution of pixel BMD change after 24 months is shown for (a) composite-beam (Charnley), (b) double-taper (Exeter), (c) triple-taper (C-stem), (d) Bi-Metric total hip replacement, and (e) ASR hip resurfacing prosthesis designs, respectively.

Figure 4: FDR q-value maps after 24 months. The significance of pixel BMD changes is quantitated using the FDR analysis at each pixel. The corresponding q-values are shown for (a) composite-beam (Charnley), (b) double-taper (Exeter), (c) triple-taper (C-stem), (d) Bi-Metric total hip replacement, and (e) ASR hip resurfacing prosthesis designs, respectively. All pixels with $q \leq 0.05$ are declared as significant bone remodeling events in this study.

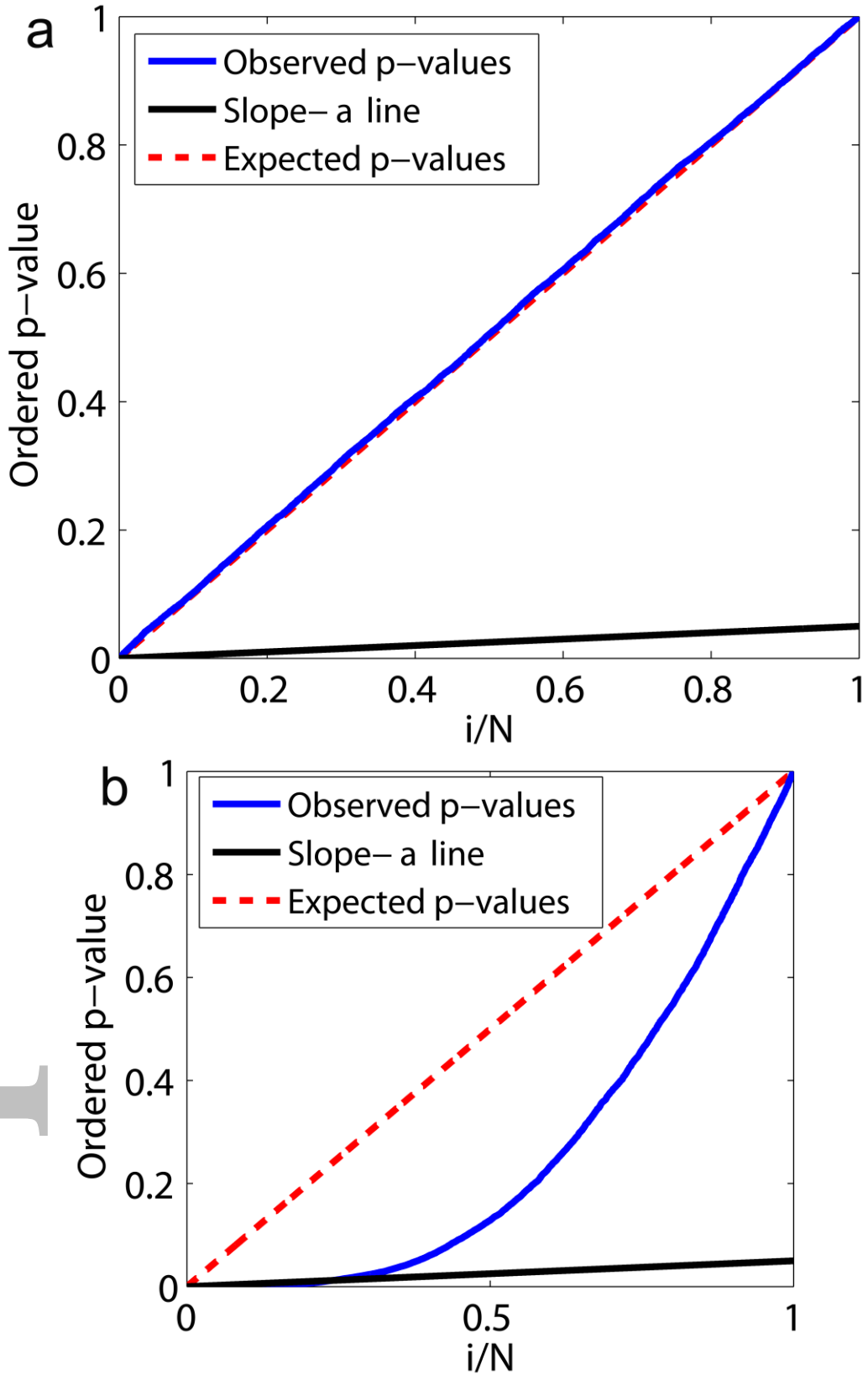

Figure 1

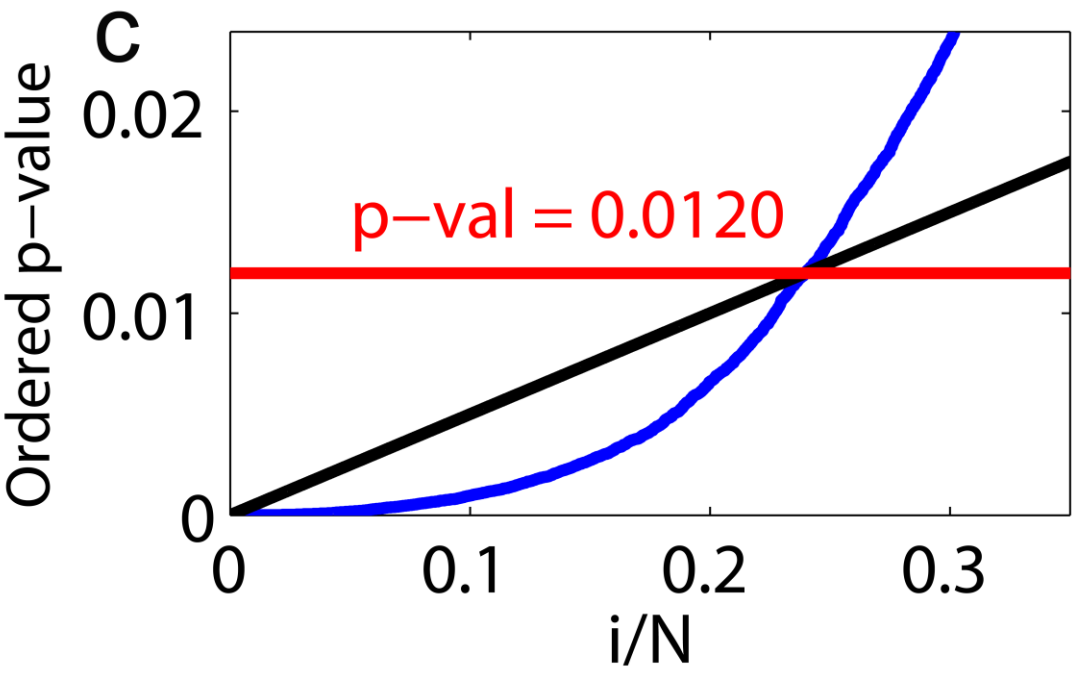

Figure 1

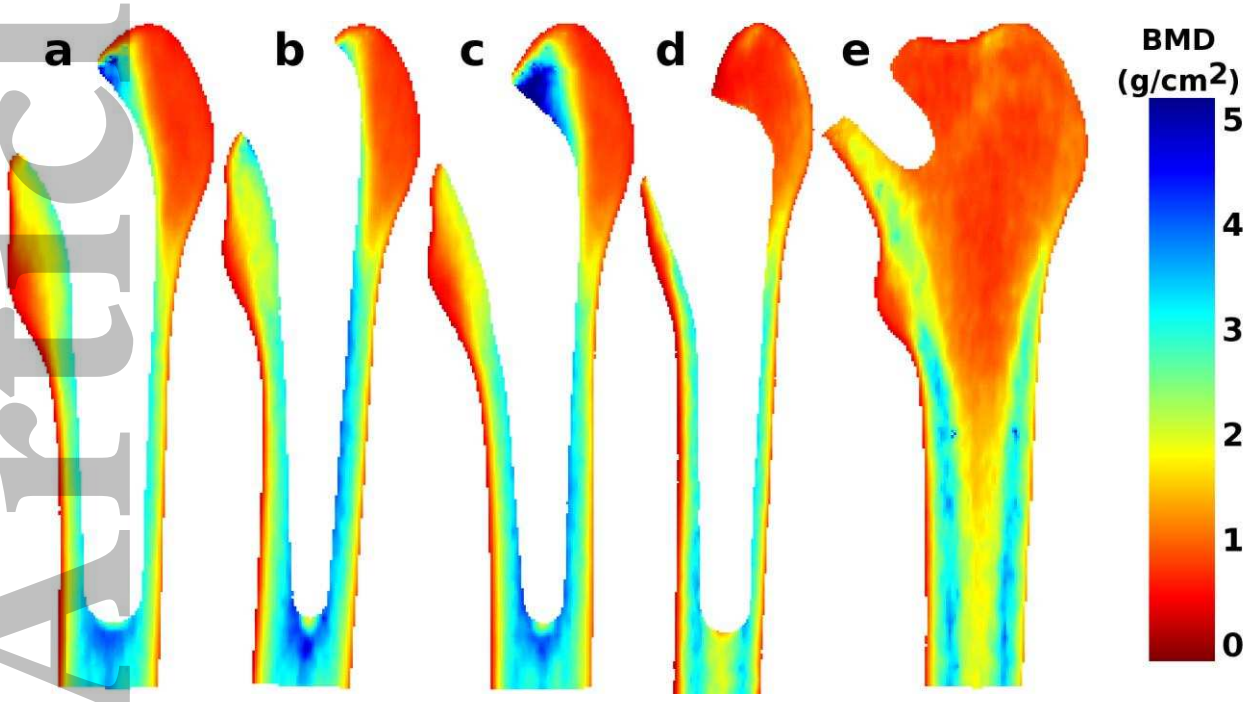

Figure 2

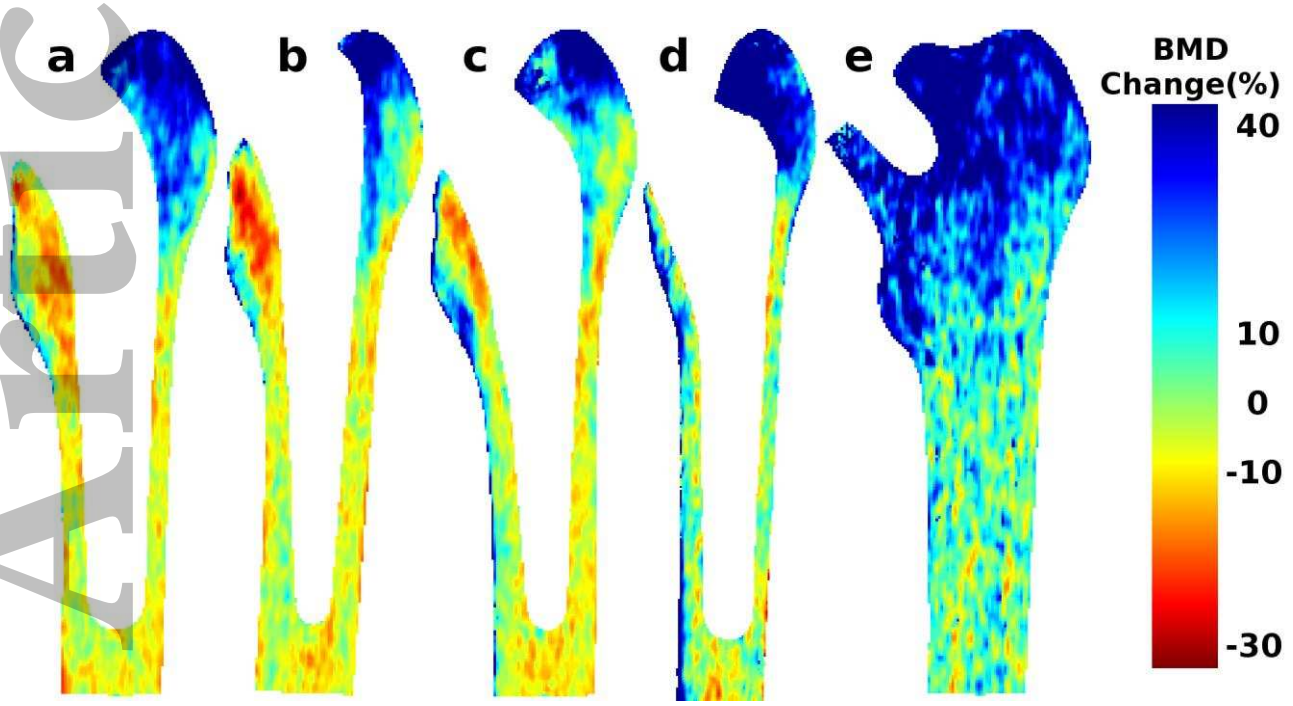

Figure 3

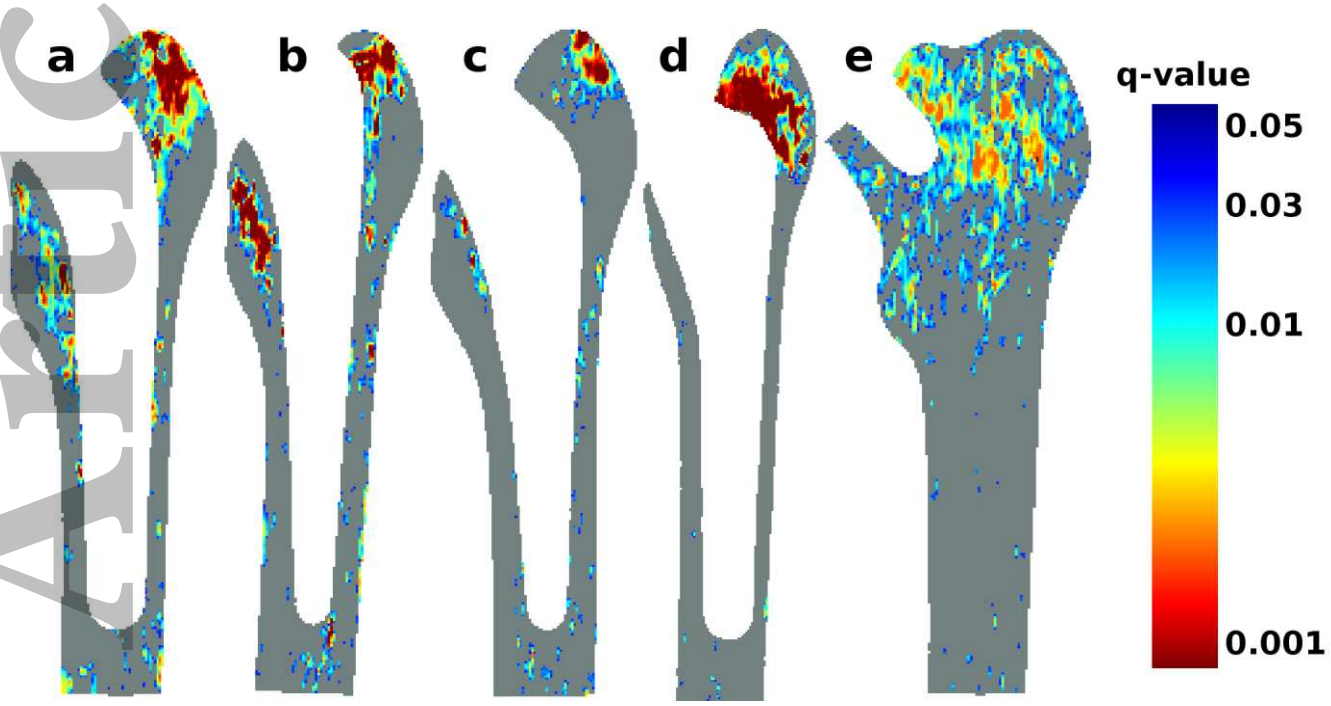

Figure 4